Chapter 1

Graphene and Active Metamaterials: Theoretical Methods and Physical Properties

Marios Mattheakis, Giorgos P. Tsironis and Efthimios Kaxiras

Additional information is available at the end of the chapter

http://dx.doi.org/10.5772/67900

Abstract

The interaction of light with matter has triggered the interest of scientists for a long time. The area of plasmonics emerges in this context through the interaction of light with valence electrons in metals. The random phase approximation in the long wavelength limit is used for analytical investigation of plasmons in three-dimensional metals, in a two-dimensional electron gas, and finally in the most famous two-dimensional semimetal, namely graphene. We show that plasmons in bulk metals as well as in a two-dimensional electron gas originate from classical laws, whereas quantum effects appear as non-local corrections. On the other hand, graphene plasmons are purely quantum modes, and thus, they would not exist in a "classical world." Furthermore, under certain circumstances, light is able to couple with plasmons on metallic surfaces, forming a surface plasmon polariton, which is very important in nanoplasmonics due to its subwavelength nature. In addition, we outline two applications that complete our theoretical investigation. First, we examine how the presence of gain (active) dielectrics affects surface plasmon polariton properties and we find that there is a gain value for which the metallic losses are completely eliminated resulting in lossless plasmon propagation. Second, we combine monolayers of graphene in a periodic order and construct a plasmonic metamaterial that provides tunable wave propagation properties, such as epsilon-near-zero behavior, normal, and negative refraction.

Keywords: random phase approximation, graphene, gain dielectrics, plasmonic metamaterial

1. Introduction

The interaction of light with matter has triggered the interest of scientists for a long time. The area of plasmonics emerges in this context through the interaction of light with electrons in

metals, while a plasmon is the quantum of the induced electronic collective oscillation. In three-dimensional (3D) metals as well as in a two-dimensional electron gas (2DEG), the plasmon arises classically through a depolarized electromagnetic field generated through Coulomb long-range interaction of valence electrons and crystal ions [1]. Under certain circumstances, light is able to couple with plasmons on metallic surfaces, forming a surface plasmon polariton (SPP) [2–4]. The SPPs are very important in nanoplasmonics and nanodevices, due to their subwavelength nature, that is, because their spatial scale is smaller than that of corresponding free electromagnetic modes. In addition to classical plasmons, purely quantum plasmon modes exist in graphene, the famous two-dimensional (2D) semimetal. Since we need the Dirac equation to describe the electronic structure of graphene, the resulting plasmons are purely quantum objects [5–8]. As a consequence, graphene is quite special from this point of view, possessing exceptional optical properties, such as ultra-subwavelength plasmons stemming from the specifics of the light-matter interaction [7–10].

In this chapter, we present basic properties of plasmons, both from a classical standpoint but also quantum mechanically using the random phase approximation approach. Plasmons in 3D metals as well as in 2DEG originate from classical laws, whereas quantum effects appear as non-local corrections [11–13]. In addition, we point out the fundamental differences between volume (bulk), surface, and two-dimensional plasmons. We show that graphene plasmons are a purely quantum phenomenon and that they would not exist in a "classical world." We then outline two applications that complete our theoretical investigation. First, we examine how the presence of gain (active) dielectrics affects SPP properties and we find that there is a gain value for which the metallic losses are completely eliminated resulting in lossless SPP propagation [3]. Second, we combine monolayers of graphene in a periodic order and construct a plasmonic metamaterial that provides tunable wave propagation properties, such as epsilon-near-zero behavior, normal, and negative refraction [9].

2. Volume and surface plasmons in three-dimensional metals

2.1. Free collective oscillations: plasmons

Plasma is a medium with equal concentration of positive and negative charges, of which at least one charge type is mobile [1]. In a classical approach, metals are considered to form plasma made of ions and electrons. The latter are only the valence electrons that do not interact with each other forming an ideal negatively charged free electron gas [1, 14]. The positive ions, that is, atomic nuclei, are uniformly distributed forming a constant background of positive charge. The background positive charge is considered to be fixed in space, and as a result, it does not respond to any electronic fluctuation or any external field while the electron gas is free to move. In equilibrium, the electron density (plasma sea) is also distributed uniformly at any point preserving the overall electrical neutrality of the system. Metals support free and collective longitudinal charge oscillation with well-defined natural frequency, called the plasma frequency ω_p. The quanta of these charge oscillations are *plasmons*, that is, quasi-particles with energy $E_p = \hbar\omega_p$, where $\hbar$ is the reduced Plank constant.

We assume a plasma model with electron (and ion) density n. A uniform charge imbalance δn is established in the plasma by displacing uniformly a zone of electrons (e.g., a small slab in Cartesian coordinates) by a small distance $\mathbf{x}$ (**Figure 1**). The uniform displacement implies that all electrons oscillate in phase [2]; this is compatible with a long wavelength approximation ($\lambda_p/\alpha \to \infty$, where λ_p is the plasmon wavelength and α is the crystal lattice constant); in this case, the associated wavenumber $|\mathbf{q}|$ (**Figure 1(b)**) is very small compared with Fermi wavenumber k_F, viz. $q/k_F \to 0$ [7]. Longitudinal oscillations including finite wave vector $\mathbf{q}$ will be taken into account later in the context of quantum mechanics. The immobilized ions form a constant charge density indicated by en, where e is the elementary charge. Let $\mathbf{x}(t)$ denote the position of the displaced electronic slab at time t with charge density given by $-e\delta n(t)$. Due to the electron displacement, an excess positive charge density is created that is equal to $e\delta n(t)$, which in equilibrium, $\delta n = 0$, reduces to zero. Accordingly, an electric field is generated and interacts with the positive background via Coulomb interaction, forcing the electron cloud to move as a whole with respect to the immobilized ions, forming an electron density oscillation, that is, the plasma oscillation. The polarized electric field is determined by the first Maxwell equation as

$$\nabla \cdot \mathbf{E} = 4\pi e\delta n, \tag{1}$$

in CGS units.[1] The displacement $\mathbf{x}(t)$ in the electronic gas produces an electric current density $\mathbf{J} = -e(n+\delta n)\dot{\mathbf{x}} \approx -en\dot{\mathbf{x}}$ (since $\delta n/n \to 0$), related to the electron charge density via the continuity equation $\nabla \cdot \mathbf{J} = -e\partial_t \delta n$. After integration in time, we obtain

$$\delta n = n\nabla \cdot \mathbf{x} \tag{2}$$

Combining Eqs. (1) and (2), we find the electric field that is induced by the electron charge displacement, that is,

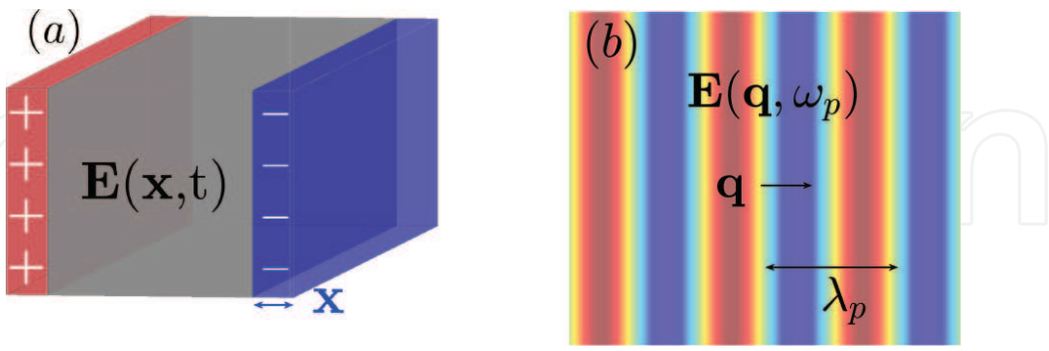

Figure 1. (a) A charge displacement is established by displacing uniformly a slab of electrons at a small distance $\mathbf{x}$, creating a polarized electric field in the solid. (b) A plasma longitudinal oscillation electric field in the bulk of a solid. The arrow indicates the direction of displacement of electrons and of the wavevector $\mathbf{q}$, while the double-faced arrow shows the plasmon wavelength λ_p.

[1]For SI units, we make the substitution $1/\varepsilon_0 = 4\pi$.

$$\mathbf{E} = 4\pi e n \mathbf{x}. \tag{3}$$

Newtonian mechanics states that an electron with mass m in an electric field $\mathbf{E}$ obeys the equation $m\ddot{\mathbf{x}} = -e\mathbf{E}$, yielding finally the equation of motion

$$m\ddot{\mathbf{x}} + 4\pi e^2 n \mathbf{x} = 0, \tag{4}$$

indicating that electrons form a collective oscillation with plasma frequency

$$\omega_p(0) = \sqrt{\frac{4\pi e^2 n}{m}}. \tag{5}$$

where $\omega_p(0) \equiv \omega_p(\mathbf{q} = 0)$. The energy $E_p = \hbar\omega_p$ is the minimum energy necessary for exciting a plasmon. Typical values of plasmon energy E_p at metallic densities are in the range of $2 - 20$ eV.

Having shown that an electron gas supports free and collective oscillation modes, we proceed to investigate the dynamical dielectric function $\varepsilon(\mathbf{q}, \omega)$ of the free electron gas. The dielectric function is the response of the electronic gas to an external electric field and determines the electronic properties of the solid [1, 11, 15]. We consider an electrically neutral homogeneous electronic gas and introduce a weak space-time-varying external charge density $\rho_{\text{ext}}(\mathbf{x},t)$ [14]. Our goal is to investigate the longitudinal response of the system as a result of the external perturbation. In free space, the external charge density produces an electric displacement field $\mathbf{D}(\mathbf{x},t)$ determined by the divergence relation $\nabla \cdot \mathbf{D} = 4\pi\rho_{\text{ext}}$. Moreover, the system responds and generates additional charges (induced charges) with density $\rho_{\text{ind}}(\mathbf{x},t)$ creating a polarization field $\mathbf{P}(\mathbf{x},t)$ defined by the expression $\nabla \cdot \mathbf{P} = -\rho_{\text{ind}}$ [1]. Because of the polarization, the total charge density inside the electron gas will be $\rho_{\text{tot}} = \rho_{\text{ext}} + \rho_{\text{ind}}$, leading to the screened electric field $\mathbf{E}$, determined by $\nabla \cdot \mathbf{E} = 4\pi\rho_{\text{tot}}$. The fundamental relation $\mathbf{D} = \mathbf{E} + 4\pi\mathbf{P}$ is derived after combining the aforementioned field equations.

The dielectric function is introduced as the linear optical response of the system. According to the linear response theory and taking into account the non-locality in time and space [2, 14], the total field depends linearly on the external field, if the latter is weak. In the most general case, we have

$$\mathbf{D}(\mathbf{x}, t) = \int d\mathbf{x}' \int_{-\infty}^{\infty} dt' \varepsilon(\mathbf{x} - \mathbf{x}', t - t')\mathbf{E}(\mathbf{x}', t'), \tag{6}$$

where we have implicitly assumed that all length scales are significantly larger than the crystal lattice, ensuring homogeneity. Thence, the response function depends only on the differences between spatial and temporal coordinates [2, 8]. In Fourier space, the convolutions turn into multiplications and the fields are decomposed into individual plane-wave components of the wavevector $\mathbf{q}$ and angular frequency ω. Thus, in the Fourier domain, Eq. (6) reads

$$\mathbf{D}(\mathbf{q}, \omega) = \varepsilon(\mathbf{q}, \omega)\mathbf{E}(\mathbf{q}, \omega). \tag{7}$$

For notational convenience, we designate the Fourier-transformed quantities with the same symbol as the original while they differ in the dependent variables. The Fourier transform of

an arbitrary field $\mathbf{F}(\mathbf{r},t)$ is given by $\mathbf{F}(\mathbf{r},t) = \int \mathbf{F}(\mathbf{q},\omega)e^{\mathrm{i}(\mathbf{q}\cdot\mathbf{r}-\omega t)}d\mathbf{q}dt$ where ω, $\mathbf{q}$ represent the Fourier transform quantities. Hence, the Fourier transform of the divergence equations of $\mathbf{D}$ and $\mathbf{E}$ yields

$$-\mathrm{i}\mathbf{q}\cdot\mathbf{D}(\mathbf{q},\omega) = 4\pi\rho_{\mathrm{ext}}(\mathbf{q},\omega) \tag{8}$$

$$-\mathrm{i}\mathbf{q}\cdot\mathbf{E}(\mathbf{q},\omega) = 4\pi\rho_{\mathrm{tot}}(\mathbf{q},\omega). \tag{9}$$

In longitudinal oscillations, the electron displacement field is in the direction of $\mathbf{q}$ (**Figure 1(b)**), thus, $\mathbf{q}\cdot\mathbf{D} = qD$ and $\mathbf{q}\cdot\mathbf{E} = qE$, where $D(\mathbf{q},\omega)$ and $E(\mathbf{q},\omega)$ refer to longitudinal fields. Combining Eqs. (7)–(9) yields

$$\rho_{\mathrm{tot}}(\mathbf{q},\omega) = \frac{\rho_{\mathrm{ext}}(\mathbf{q},\omega)}{\varepsilon(\mathbf{q},\omega)}. \tag{10}$$

Interestingly enough, in the absence of external charges, $\rho_{\mathrm{ext}}(\mathbf{q},\omega) = 0$, Eq. (10) states that nonzero amplitudes of charge oscillation exist, that is, $\rho_{\mathrm{tot}}(\mathbf{q},\omega) \neq 0$, under the condition

$$\varepsilon(\mathbf{q},\omega) = 0. \tag{11}$$

In other words, in the absence of any external perturbation, free collective charge oscillations exist with dispersion relation $\omega(\mathbf{q})$ that satisfies condition (11). These are plasmon modes, and consequently, Eq. (11) is referred as *plasmon condition*. Furthermore, condition (11) leads to $\mathbf{E} = -4\pi\mathbf{P}$, revealing that at plasmon frequencies the electric field is a pure depolarization field [1, 2].

We note that due to their longitudinal nature, plasmon waves cannot couple to any transverse wave such as electromagnetic waves; as a result, volume plasmons cannot be excited by light. On the other hand, moving charged particles can be used for exciting plasmons. For instance, an electron beam passing through a thin metal excites plasmons by transferring part of its energy to the plasmon excitation. As a result, plasmons do not decay directly via electromagnetic radiation but only through energy transfer to electron-hole excitation (Landau damping) [2, 8, 14].

2.2. Dynamical dielectric function

Based on the plasmon condition (11), the problem has been reduced in the calculation of the dynamical dielectric function $\varepsilon(\mathbf{q},\omega)$. Further investigation of $\varepsilon(\mathbf{q},\omega)$ reveals the plasmon dispersion relation as well as the Landau-damping regime, that is, where plasmons decay very fast exciting electron-hole pairs [8]. Classically, in the long wavelength limit, the dielectric response $\varepsilon(0,\omega)$ can be calculated in the context of the plasma model [1, 11]. Let us consider the plasma model of Eq. (4) subjected to a weak and harmonic time-varying external field $\mathbf{D}(t) = \mathbf{D}(\omega)e^{-\mathrm{i}\omega t}$; Eq. (4) is modified to read

$$m\ddot{\mathbf{x}}(t) + 4\pi e^2 n\mathbf{x}(t) = -e\mathbf{D}(t). \tag{12}$$

Assuming also a harmonic in time electron displacement, that is, $\mathbf{x}(t) = \mathbf{x}(\omega)e^{-\mathrm{i}\omega t}$, the Fourier transform of Eq. (12) yields

$$(-m\omega^2 + 4\pi e^2 n)\mathbf{x}(\mathbf{q},\omega) = -e\mathbf{D}(\mathbf{q},\omega). \tag{13}$$

Introducing Eq. (3) in Eq. (13) and using the relation (7), we derive the spatially local dielectric response

$$\varepsilon(0,\omega) = 1 - \frac{\omega_p(0)^2}{\omega^2}, \tag{14}$$

where the plasma frequency $\omega_p(0)$ is defined in Eq. (5). Eq. (14) verifies that the plasmon condition (11) is satisfied at the plasma frequency. The dielectric function (14) coincides with the Drude model permittivity.

Further investigation of the dynamical dielectric function can be performed using quantum mechanics. An explicit form of $\varepsilon(\mathbf{q},\omega)$ including screening effect has been evaluated in the context of the *random phase approximation* (RPA) [8, 12–14] and is given by

$$\varepsilon(\mathbf{q},\omega) = 1 - v_c(\mathbf{q})\chi_0(\mathbf{q},\omega) \tag{15}$$

where $v_c(\mathbf{q})$ is the Fourier transform of the Coulomb potential and $\chi_0(\mathbf{q},\omega)$ is the polarizability function, known as Lindhard formula [8, 12–14]. The Coulomb potential in two and three dimensions, respectively, reads

$$v_c(\mathbf{q}) = \begin{cases} \dfrac{2\pi e^2}{|\mathbf{q}|\varepsilon_b} & \text{(2D)} \\ \dfrac{4\pi e^2}{|\mathbf{q}|^2\varepsilon_b} & \text{(3D)} \end{cases} \tag{16}$$

where ε_b represents the background lattice dielectric constant of the system.

In RPA approach, the dynamical conductivity $\sigma(\mathbf{q},\omega)$ reads [8]

$$\sigma = \frac{\mathrm{i}\omega e^2}{q^2}\chi_0(\mathbf{q},\omega), \tag{17}$$

revealing the fundamental relation between $\varepsilon(\mathbf{q},\omega)$ and $\sigma(\mathbf{q},\omega)$ that also depends on system dimensions; we have finally

$$\varepsilon(\mathbf{q},\omega) = 1 + \mathrm{i}\frac{q^2 v_c}{\omega e^2}\sigma(\mathbf{q},\omega). \tag{18}$$

In the random phase approximation, the most important effect of interactions is that they produce electronic screening, while the electron-electron interaction is neglected. The polarizability of a non-interacting electron gas is represented by Lindhard formula as follows:

$$\chi_0(\mathbf{q},\omega) = -\frac{2}{V}\sum_{\mathbf{k}} \frac{f(\epsilon_{\mathbf{k}+\mathbf{q}}) - f(\epsilon_{\mathbf{k}})}{\hbar\omega - (\epsilon_{\mathbf{k}+\mathbf{q}} - \epsilon_{\mathbf{k}}) + \mathrm{i}\hbar\eta} \tag{19}$$

where factor 2 is derived by spin degeneracy (summation over the two possible values of spin $s = \uparrow,\downarrow$) [8, 13, 14]. The summation is over all the wavevectors $\mathbf{k}$, V is the volume, $i\hbar\eta$ represents a small imaginary number to be brought to zero after the summation, and $\epsilon_{\mathbf{k}}$ is the kinetic energy for the wave vector $\mathbf{k}$. The carrier distribution f is given by Fermi-Dirac distribution $f(\epsilon_{\mathbf{k}}) = \left(\exp\left[\beta(\epsilon_{\mathbf{k}} - \mu)\right] + 1\right)^{-1}$, where μ is the chemical potential and $\beta = 1/k_B T$ with Boltzmann's constant denoted by k_B and T is the absolute temperature. Equation (19) describes processes in which a particle in state $\mathbf{k}$, which is occupied with probability $f(\epsilon_{\mathbf{k}})$, is scattered into state $\mathbf{k} + \mathbf{q}$, which is empty with probability $1 - f(\epsilon_{\mathbf{k}+\mathbf{q}})$. Eqs. (15)–(19) consist of the basic equations for a detailed investigation of charge density fluctuations and the screening effect, electron-hole pair excitation, and plasmons. With respect to condition (11), the roots of Eq. (15) determine the plasmon modes. Moreover, the poles of χ_0 account for electron-hole pair excitation defining the Plasmon-damping regime [12–14].

For an analytical investigation, we split the summation of Eq. (19) in two parts. We make an elementary change of variables $\mathbf{k} + \mathbf{q} \to -\mathbf{k}$, in the term that includes $f(\epsilon_{\mathbf{k}+\mathbf{q}})$, and assume that the kinetic energy is symmetric with respect to the wavevector, that is, $\epsilon_{\mathbf{k}} = \epsilon_{-\mathbf{k}}$. Therefore, formula (19) yields

$$\chi_0(\mathbf{q},\omega) = \frac{2}{V}\left(\sum_{\mathbf{k}} \frac{f(\epsilon_{\mathbf{k}})}{\hbar z - (\epsilon_{\mathbf{k}+\mathbf{q}} - \epsilon_{\mathbf{k}})} - \sum_{\mathbf{k}} \frac{f(\epsilon_{\mathbf{k}})}{\hbar z + (\epsilon_{\mathbf{k}+\mathbf{q}} - \epsilon_{\mathbf{k}})}\right) \tag{20}$$

where $z = \omega + i\eta$. At zero temperature, the chemical potential is equal to Fermi energy, that is, $\mu = E_F$ [8, 11, 14], and the Fermi-Dirac distribution is reduced to Heaviside step function, thus, $f(\epsilon_{\mathbf{k}})|_{T=0} = \Theta(E_F - \epsilon_{\mathbf{k}})$. The kinetic energy of each electron of mass m in state $\mathbf{k}$ is given by

$$\epsilon_{\mathbf{k}} = \frac{\hbar^2 |\mathbf{k}|^2}{2m}, \tag{21}$$

hence

$$\epsilon_{\mathbf{k}+\mathbf{q}} - \epsilon_{\mathbf{k}} = \frac{\hbar^2}{2m}(|\mathbf{q}|^2 + 2\mathbf{k}\cdot\mathbf{q}). \tag{22}$$

At zero temperature, because of the Heaviside step function, the only terms that survive in summation (20) are those with $|\mathbf{k}| < k_F$, where k_F is the Fermi wavenumber and related to Fermi energy by equation (21) as $k_F = (2mE_F/\hbar^2)^{1/2}$. Subsequently, we obtain for the Lindhard formula

$$\chi_0(\mathbf{q},\omega) = \frac{4}{V}\sum_{|\mathbf{k}|<k_F} \frac{\epsilon_{\mathbf{k}+\mathbf{q}} - \epsilon_{\mathbf{k}}}{(\hbar z)^2 - (\epsilon_{\mathbf{k}+\mathbf{q}} - \epsilon_{\mathbf{k}})^2} \tag{23}$$

Summation turns into integration by using $V^{-1}\sum_{|\mathbf{k}|}(\ldots) \to (2\pi)^{-3}\int d^3\mathbf{k}(\ldots)$, hence

$$\chi_0(\mathbf{q},\omega) = \frac{4}{(2\pi)^3}\int d^3\mathbf{k}\frac{\epsilon_{\mathbf{k}+\mathbf{q}} - \epsilon_{\mathbf{k}}}{(\hbar z)^2 - (\epsilon_{\mathbf{k}+\mathbf{q}} - \epsilon_{\mathbf{k}})^2} \tag{24}$$

where the imaginary part in z guarantees the convergence of the integrals around the poles $\hbar\omega = \pm(\epsilon_{\mathbf{k}+\mathbf{q}} - \epsilon_{\mathbf{k}})$. The poles of χ_0 determine the Landau-damping regime where plasmons decay into electron-hole pairs excitation. In particular, the damping regime is a continuum bounded by the limit values of $(\epsilon_{\mathbf{k}+\mathbf{q}} - \epsilon_{\mathbf{k}})$; $\mathbf{k}$ takes its maximum absolute value $|\mathbf{k}| = k_F$ and the inner product takes the extreme values $k_F\,\hat{\mathbf{k}}\cdot\mathbf{q} = \pm k_F|\mathbf{q}|$.

$$\frac{\hbar q}{2m}(q - 2k_F) < \omega < \frac{\hbar q}{2m}(q + 2k_F), \tag{25}$$

where $q = |\mathbf{q}|$. The Landau-damping continuum (electron-hole excitation regime) is demonstrated in **Figure 2** by the shaded area.

Introducing relation (22) into Eq. (24) and changing to spherical coordinates (r,θ,ϕ), where $r = |\mathbf{k}|$ and θ are the angle between $\mathbf{k}$ and $\mathbf{q}$, we obtain

$$\chi_0(q,\omega) = \frac{2k_F^4 q}{(2\pi)^3 m z^2}\int_0^{2\pi} d\phi \int_0^1 dx\, x^2 \int_0^{\pi} d\theta \frac{\left(\frac{q}{k_F} + 2x\cos\theta\right)\sin\theta}{1 - \left(\frac{v_F q}{z}\right)^2\left(\frac{q}{2k_F} + x\cos\theta\right)^2}. \tag{26}$$

where $x = r/k_F$ is a dimensionless variable and $v_F = \hbar k_F/m$ is the Fermi velocity. In the non-static ($\omega \gg v_F q$) and long wavelength ($q \ll k_F$) limits, we can expand the integral in a power series of q. Keeping up to q^3 orders, we evaluate integral (26) and set the imaginary part of z zero, that is, $z = \omega$. That leads to a third-order approximation polarizability function

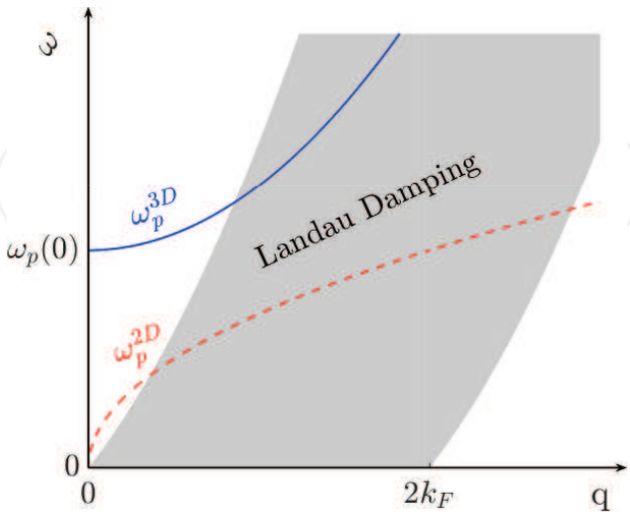

Figure 2. Dispersion relation of plasmons in the bulk of three-dimensional solid (blue solid line) and in two-dimensional electron gas (dashed red curve) plasmons. The shaded region demonstrates the Landau-damping regime where plasmons decay to electron-hole pairs excitation.

$$\chi_0(q,\omega) = \frac{k_F^3 q^2}{3\pi^2 m\omega^2}\left(1 + \frac{3v_F^2 q^2}{5\omega^2}\right), \tag{27}$$

which, in turn, yields the dielectric function by using formula (14) and the three-dimensional Coulomb interaction (16), hence

$$\varepsilon(q \to 0,\omega) = 1 - \frac{\omega_p(0)^2}{\omega^2}\left(1 + \frac{3}{5}\left(\frac{v_F q}{\omega}\right)^2\right), \tag{28}$$

where vacuum is assumed as background ($\varepsilon_d = 1$) and we use the relation 0 [1, 15] where n is the electron density. The result (28) is reduced to simple Drude dielectric function (14) for $q = 0$.

The plasmon condition (11) determines the q-dependent plasmon dispersion relation $\omega_p(q)$. Demanding $\varepsilon(q,\omega) = 0$, Eq. (28) yields approximately

$$\omega_p(q) \approx \omega_p(0)\left(1 + \frac{3}{10}\left(\frac{v_F q}{\omega_p(0)}\right)^2\right). \tag{29}$$

Interestingly enough, the leading term of plasma frequency (29) does not include any quantum quantity, such as v_F, which appears as non-local correction in sub-leading terms. That reveals that plasmons in 3D metals are purely classical modes. Moreover, a gap, that is, $\omega_p(0)$, appears in the plasmon spectrum of three-dimensional metals. The plasmon dispersion relation (29) is shown in **Figure 2**.

In the random phase approximation, the electrons do not scatter, that is, collision between electrons and crystal impurities is not taken into account. As a consequence, the dielectric function is calculated to be purely real; this is nevertheless an unphysical result as can be seen clearly at zero frequency where the dielectric function is not well defined, that is, $\varepsilon(q,0) = \infty$. The problem is cured by introducing a relaxation time τ in the denominator of the dielectric function as follows:

$$\varepsilon(q \to 0,\omega) = 1 - \frac{\omega_p^2(q)}{\omega(\omega + \mathrm{i}/\tau)} \tag{30}$$

We can phenomenologically prove expression (30) by using the simple plasma model. In particular, we modify the equation of motion (12) to a damped-driven harmonic oscillator by assuming that the motion of electron is damped via collisions occurring with a characteristic frequency $\gamma = 1/\tau$ [2]; this approach immediately leads to the dielectric response (30). Typically values of relaxation time τ are of the order 10^{-14} s, at room temperature. The relaxation time is determined experimentally. In the presence of τ, the dielectric function (15) is well defined at $\omega = 0$, where the real part of permittivity has a peak with width τ^{-1} known as *Drude peak*. Furthermore, it can be shown that equation (30) satisfies the Kramers-Kronig relations (sum rules) [1, 14, 15].

2.3. Surface plasmon polariton

A new guided collective oscillation mode called *surface plasmon* arises in the presence of a boundary. Surface plasmon is a surface electromagnetic wave that propagates along an interface between a conductor (metal) and an insulator (dielectric). This guided mode couples to electromagnetic waves resulting in a polariton. Surface plasmon polaritons (SPPs) occur at frequencies close to but smaller than plasma frequency. These surface modes show exceptional properties for applications of nanophotonics, specifically they constitute a class of nanophotonics themselves, namely nanoplasmonics. The basic property is the subwavelength nature, that is, the wavelength of SPPs is smaller than electromagnetic radiation at the same frequency and in the same medium [2, 3, 9].

Let us consider a waveguide formed by a planar interface at $z = 0$ consisting of two semi-infinite nonmagnetic media (permeability $\mu = 1$) with dielectric functions ε_1 and ε_2 as **Figure 3a** denotes. The dielectric functions are assumed to be local in space (non-$q-$dependent) and nonlocal in time (ω dependence), hence $\varepsilon_{1,2} = \varepsilon_{1,2}(\omega)$. Assuming harmonic in time dependence in the form $\mathbf{u}(\mathbf{r},t) = \mathbf{u}(\mathbf{r})e^{-i\omega t}$, the Maxwell equations (in CGS units) in the absence of external charges and currents read

$$\nabla \cdot (\varepsilon_j \mathbf{E}_j) = 0 \qquad \nabla \times \mathbf{E}_j = ik_0 \mathbf{H}_j \tag{31}$$

$$\nabla \cdot (\mathbf{H}_j) = 0 \qquad \nabla \times \mathbf{H}_j = -i\varepsilon_j k_0 \mathbf{E}_j \tag{32}$$

where $k_0 = \omega/c$ is the free space wavenumber and the index j denotes the media as $j = 1$ for $z < 0$ and $j = 2$ for $z > 0$. Combining Eqs. (31) and (32), the fields are decoupled into two separate Helmholtz equations [2, 4] as

$$\left[\nabla^2 + k_0^2 \varepsilon_j\right] \begin{pmatrix} \mathbf{E}_j(\mathbf{r}) \\ \mathbf{H}_j(\mathbf{r}) \end{pmatrix} = 0 \tag{33}$$

where $\mathbf{r} = (x,y,z)$. For simplicity, let us assume surface electromagnetic waves propagating along one direction, chosen to be the x direction (**Figure 3b**), and show no spatial variations in the perpendicular in-plane direction, hence $\partial_y \mathbf{u} = 0$. Under this assumption, we are seeking

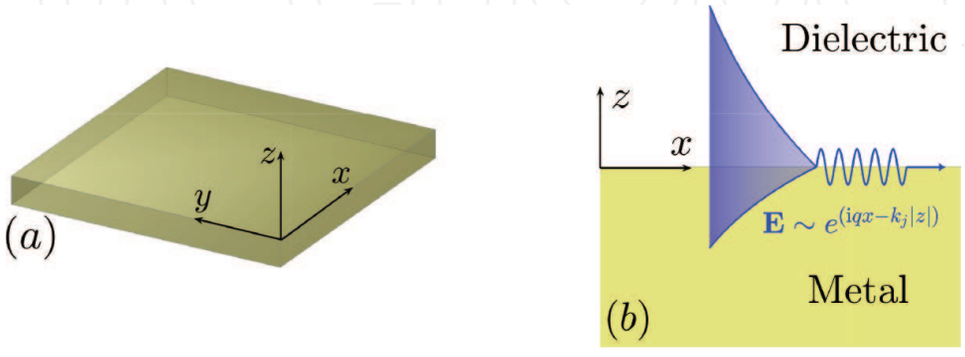

Figure 3. A planar interface is formed between a metal and a dielectric where surface plasmon polaritons (SPPs) propagate in (a) three- and (b) two-dimensional representation. (b) A schematic illustration of the SPP field.

electromagnetic waves of the form $\boldsymbol{\psi}_j(\mathbf{r}) = \boldsymbol{\psi}_j(z)e^{\mathrm{i}q_j x}$, where $\boldsymbol{\psi}_j = (\mathbf{E}_j,\mathbf{H}_j)^T$ and q will be the plasmon propagation constant. Substituting the aforementioned ansatz into Helmholtz equation (33), we obtain the guided electromagnetic modes equation [2]

$$\left[\frac{\partial^2}{\partial z^2} + (k_0^2\varepsilon_j - q_j^2)\right]\begin{pmatrix}\mathbf{E}_j(z)\\ \mathbf{H}_j(z)\end{pmatrix} = 0. \tag{34}$$

Surface waves are waves that have been trapped at the interface ($z = 0$) and decay exponentially away from it $\left(\boldsymbol{\psi}_j(z) \sim e^{-\kappa_j|z|} \text{for } k_j > 0\right)$. Consequently, propagating wave solutions along z is not desired. In turn, we derive the *surface wave condition*

$$\kappa_j = \sqrt{q_j^2 - k_0^2\varepsilon_j} \in \mathbb{R}. \tag{35}$$

In order to determine the spatial field profiles and the SPP dispersion relation, we need to find explicit expressions for each field component of **E** and **H**. This can be achieved by solving the curl equations (31) and (32), which naturally lead to two self-consistent set of coupled governing equations. Each set corresponds to one of the fundamental polarizations, namely transverse magnetic (TM) (*p*-polarized waves) and transverse electric (TE) (*s*-polarized waves), hence

Transverse magnetic (TM)		**Transverse electric (TE)**	
E_{jz}	$= -\frac{q_j}{k_0\varepsilon_j}H_{jy}$	H_{jz}	$= \frac{q}{k_0}E_{jy}$
E_{jx}	$= -\frac{\mathrm{i}}{k_0\varepsilon_j}\frac{\partial}{\partial z}H_{jy}$	H_{jx}	$= \frac{\mathrm{i}}{k_0}\frac{\partial}{\partial z}E_{jy}$
$\frac{\partial^2}{\partial z^2}H_{jy}$	$-(q_j^2 - k_0^2\varepsilon_j)H_{jy} = 0$	$\frac{\partial^2}{\partial z^2}E_{jy}$	$-(q_j^2 - k_0^2\varepsilon_j)E_{jy} = 0$

We focus on transverse magnetic (TM) polarization, in which the magnetic field **H** is parallel to the interface. Since the planar interface extends along (x,y) plane, the TM fields read $\mathbf{E}_j = (E_{jx}, 0, E_{jz})$ and $\mathbf{H}_j = (0, H_{jy}, 0)$. Solving the TM equations for surface waves, we obtain for each half plane

$$\begin{gathered} z < 0 \quad (j = 1) \\ H_y = A_1 e^{\mathrm{i}q_1 x} e^{k_1 z} \end{gathered} \tag{36}$$

$$E_x = -\frac{\mathrm{i}k_1 A_1}{k_0\varepsilon_1} e^{\mathrm{i}q_1 x} e^{k_1 z} \tag{37}$$

$$E_z = -\frac{q_1 A_1}{k_0\varepsilon_1} e^{\mathrm{i}q_1 x} e^{k_1 z} \tag{38}$$

$$\begin{gathered} z > 0 \quad (j = 2) \\ H_y = A_2 e^{\mathrm{i}q_2 x} e^{-k_2 z} \end{gathered} \tag{39}$$

$$E_x = \frac{\mathrm{i}k_2 A_2}{k_0 \varepsilon_2} e^{\mathrm{i}q_2 x} e^{-k_2 z} \tag{40}$$

$$E_z = -\frac{q_2 A_2}{k_0 \varepsilon_2} e^{\mathrm{i}q_2 x} e^{-k_2 z} \tag{41}$$

where k_j is related to q_j by Eq. (35). The boundary conditions imply that the parallel to interface components of electric (E_x) and magnetic (H_y) fields must be continuous. Accordingly, we demand Eqs. (36) = (39) and Eqs. (37) = (40) at $z = 0$, hence we find the system of equations

$$\begin{pmatrix} e^{\mathrm{i}q_1 x} & -e^{\mathrm{i}q_2 x} \\ \frac{k_1}{\varepsilon_1} e^{\mathrm{i}q_1 x} & \frac{k_2}{\varepsilon_2} e^{\mathrm{i}q_2 x} \end{pmatrix} \begin{pmatrix} A_1 \\ A_2 \end{pmatrix} = 0, \tag{42}$$

which has a solution only if the determinant is zero. As an outcome, we obtain the so-called *surface plasmon polariton condition*

$$\frac{k_1}{\varepsilon_1} + \frac{k_2}{\varepsilon_2} = 0. \tag{43}$$

Condition (43) states that the interface must consist of materials with opposite signed permittivities, since surface wave condition requires the real part of both k_1 and k_2 to be non-negative numbers. For that reason, interface between metals and dielectrics may support surface plasmons, since metals show negative permittivity at frequencies smaller than plasma frequency [2]. Furthermore, boundary conditions demand the continuity of the normal to the interface electric displacement ($D_{jz} = \varepsilon_j E_{jz}$) yielding the continuity of the plasmon propagation constant $q_1 = q_2 = q$ [4]. In turn, by combining Eq. (35) with Eq. (43) we obtain the dispersion relation for the surface plasmon polariton

$$q(\omega) = \frac{\omega}{c} \sqrt{\frac{\varepsilon_1 \varepsilon_2}{\varepsilon_1 + \varepsilon_2}} \tag{44}$$

where $\varepsilon_{1,2}$ are, in general, complex functions of ω. For a metal-dielectric interface, it is more convenient to use the notation $\varepsilon_1 = \varepsilon_d$ and $\varepsilon_2 = \varepsilon_m$ for dielectric and metal permittivity, respectively. In long wavelengths, the SPP wavenumber is close to the light line in dielectric, viz. $q \simeq k_0 \sqrt{\varepsilon_d}$, and the waves are extended over many wavelengths into the dielectrics [2, 4]; these waves are known as Sommerfeld-Zenneck waves and share similarities with free surface electromagnetic modes [2]. On the other hand, at the limit $q \to \infty$, Eq. (44) asymptotically leads to the condition

$$\varepsilon_d + \varepsilon_m = 0 \tag{45}$$

indicating the *nonretarded* surface plasmon limit [4]. In the vicinity of the nonretarded limit, Eq. (35) yields $k_j \simeq q \gg k_0$. Furthermore, in the nonretarded limit the phase velocity $v_{\mathrm{ph}} = \omega/q$ is tending to zero unveiling the electrostatic nature characterized by the surface plasmon [2, 3]. As a result, at the same frequency v_{ph} is much smaller than the speed of light and, thus, the SPP

wavelength ($\lambda_{\rm sp}$) is always smaller than the light wavelength ($\lambda_{\rm ph}$), that is, $\lambda_{\rm sp} < \lambda_{\rm ph}$, revealing the subwavelength nature of surface plasmon polaritons [2, 4]. In addition, due to the fact that SPP phase velocity is always smaller than the phase velocity of propagating electromagnetic waves, SPPs cannot radiate and, hence, they are well-defined surface propagating electromagnetic waves. Demanding $q \to \infty$ in the dielectric function (30), we find the so-called *surface plasmon frequency* $\omega_{\rm sp}$, which is the upper frequency limit that SPPs occur

$$\omega_{sp} = \sqrt{\frac{\omega_p^2}{1+\varepsilon_d} - \gamma^2} \simeq \frac{\omega_p}{\sqrt{1+\varepsilon_d}}, \tag{46}$$

indicating that SPPs always occur at frequencies smaller than bulk plasmons.

If we follow the same procedure for transverse electric polarized fields, in which the electric field is parallel to interface and the only non-zero electromagnetic field components are E_y,H_x, and H_z, we will find the condition $k_1 + k_2 = 0$ [2]. This condition is satisfied only for $k_1 = k_2 = 0$ unveiling that *s*-polarized surface modes do not exist. Consequently, surface plasmon polaritons are always TM electromagnetic waves.

Due to metallic losses, SPPs decay exponentially along the interface restricting the propagation length. Mathematically speaking, losses are described by the small imaginary part in the complex dielectric function of metal $\varepsilon_m = -\varepsilon_{m'} - {\rm i}\varepsilon_m''$, where $\varepsilon_m', \varepsilon_m'' > 0$. Consequently, the SPPs propagation constant (44) becomes complex, that is, $q = q' + {\rm i}q''$, where the imaginary part accounts for losses of SPPs energy. In turn, the effective propagation length L, which shows the rate of change of the energy attenuation of SPPs [2, 3], is determined by the imaginary part ${\rm Im}[q]$ as $L^{-1} = 2{\rm Im}[q]$.

Gain materials rather than passive regular dielectrics have been used to reduce the losses in SPP propagation. Gain materials are characterized by a complex permittivity function, that is, $\varepsilon_d = \varepsilon_d' = +{\rm i}\varepsilon_d''$, with $\varepsilon_d', \varepsilon_d'' > 0$, where ε_d'' is a small number compared to ε_d' and accounts for gain. As a result, gain dielectric gives energy to the system counterbalancing the metal losses. We investigate the SPP dispersion relation (44) in the presence of gain and loss materials, and find an explicit formula for gain ε_d'' where the SPP wavenumber is reduced to real function, resulting in lossless SPPs propagation. In addition, we find an upper limit that values of gain are allowed. In this critical gain, the purely real SPP propagation constant becomes purely imaginary, destroying the SPP modes.

The dispersion relation (44) can also be written as $q = k_0 n_{\rm sp}$ [3], where $n_{\rm sp}$ is the plasmon effective refractive index given by

$$n_{sp} = \sqrt{\frac{\varepsilon_d \varepsilon_m}{\varepsilon_d + \varepsilon_m}}. \tag{47}$$

We are seeking for a gain ε_d'' such that the effective index $n_{\rm sp}$ becomes real. Substituting the complex function describing the dielectric and metal into Eq. (47), the function $n_{\rm sp}$ is written in the ordinary complex form as [3]

$$n_{sp} = \sqrt{\frac{\sqrt{x^2+y^2}+x}{2}} + \mathrm{i}\,\mathrm{sgn}(y)\sqrt{\frac{\sqrt{x^2+y^2}-x}{2}}, \tag{48}$$

where $\mathrm{sgn}(y)$ is the discontinuous signum function [3] and

$$x = \frac{\varepsilon_d'|\varepsilon_m|^2 - \varepsilon_m'|\varepsilon_d|^2}{|\varepsilon_d+\varepsilon_m|^2} \tag{49}$$

$$y = \frac{\varepsilon_d''|\varepsilon_m|^2 - \varepsilon_m''|\varepsilon_d|^2}{|\varepsilon_d+\varepsilon_m|^2} \tag{50}$$

with $|z_*|$ denoting the norm of the complex number z_*. The poles in Eqs. (49) and (50) correspond to the nonretarded surface plasmon limit (45).

Considering the plasmon effective index n_{sp} in Eq. (48) in the (x, y) plane, we observe that lossless SPP propagation $(\mathrm{Im}[n_{sp}] = \mathrm{Im}[q] = 0)$ is warranted when the conditions $y = 0$ and $x > 0$ are simultaneously satisfied. Let us point out that for $y = 0$ and $x < 0$, although the imaginary part in Eq. (48) vanishes due to the signum function, its real part becomes imaginary, that is, $n_{\mathrm{sp}} = \mathrm{i}\sqrt{|x|}$, which does not correspond to propagation waves. Solving Eq. (50) for $y = 0$ with respect to gain ε_d'' and avoiding the nonretarded limit (45), that is, $\varepsilon_d \neq -\varepsilon_m$, we obtain two exact solutions [3] as follows:

$$\varepsilon_d''\pm = \frac{|\varepsilon_m|^2}{2\varepsilon_m''}\left(1 \pm \sqrt{1-\left(\frac{2\varepsilon_d'\varepsilon_m''}{|\varepsilon_m|^2}\right)^2}\right). \tag{51}$$

Due to the fact that ε_d is real, we read from Eq. (51) that [3].

$$|\varepsilon_m|^2 \geqslant 2\varepsilon_d'\varepsilon_m''. \tag{52}$$

Using inequality (52), we read for the solution ε_{d+} of Eq. (51) that $\varepsilon''_{d+} \geqslant \varepsilon_d'$. This is a contradiction since the ε_d'' is defined to be smaller than ε_d'. Thus, ε_{d+} does not correspond to a physically relevant gain.

Solving, on the other hand, Eq. (49) for $x > 0$, with respect to the dielectric gain ε_d'', we determine a critical value ε_c distinguishing the regimes of lossless and prohibited SPP propagation [3], namely

$$\varepsilon_c = \varepsilon_d'\sqrt{\frac{|\varepsilon_m|^2}{\varepsilon_m'\varepsilon_d',} - 1}, \tag{53}$$

hence, Eq. (53) sets an upper limit in values of gain. The appearance of critical gain can be understood as follows: In Eq. (51) the gain ε_{d-} becomes equal to critical gain ε_c when $\varepsilon_d + \varepsilon_m = 0$ [3], where the last item is the nonretarded limit where $q \to \infty$. Specifically, the

surface plasmon exists when the metal is characterized by the Drude dielectric function of Eq. (30), $\varepsilon_d'' - = \varepsilon_c$ at $\omega = \omega_{sp}$, corresponding to a maximum frequency [3].

In order to represent the above theoretical findings, we use the dielectric function of Eq. (30) to calculate the SPP dispersion relation for an interface consisting of silver with $\omega_p(0) = 13.67$ PHz and $\gamma = 0.1018$ PHz, and silica glass with $\varepsilon_d' = 1.69$ and for gain $\varepsilon_d'' = \varepsilon_{d-}$ determined by Eq. (51). We represent in **Figure 3a** the SPP dispersion relation of Eq. (44) for lossless case ($\varepsilon_d'' = \varepsilon_d'' -$), where the lossless gain is denoted by the inset image in **Figure 3a**. We indicate the real and imaginary of normalized SSP dispersion q/k_p ($k_p \equiv \omega_p/c$), with respect to the normalized frequency ω/ω_p. We observe, indeed, that for $\omega < \omega_{\text{sp}}$ the imaginary part of q vanishes, whereas for $\omega > \omega_{\text{sp}}$ the SPPs wavenumber is purely imaginary. Subsequently, in the vicinity of $\omega = \omega_{\text{sp}}$ a phase transition from lossless to prohibited SPPs propagation is expected [3].

We also solve numerically the full system of Maxwell equations (31) and (32) in a two-dimensional space for transverse magnetic polarization. The numerical experiments have been performed by virtue of the multi-physics commercial software COMSOL and the frequency ω is confined in the range $[0.3\omega_p, 0.75\omega_p]$ with the integration step $\Delta\omega = 0.01\omega_p$. In the same range, the lossless gain is calculated by Eq. (51), to be $[8 \cdot 10^{-3}, 8 \cdot 10^{-2}]$. For the excitation of SPPs on the metallic surface, we use the near-field technique [2, 3, 9, 10]. For this purpose, a circular electromagnetic source of radius $R = 20$ nm has been located 100 nm above the metallic surface acting as a point source, since the wavelength λ of EM waves is much larger, that is, $\lambda >> R$ [2, 3]. In **Figure 4b**, we demonstrate, in a log-linear scale, the propagation length L, with respect to ω, subject in lossless gain ε_{d-} (blue line and open circles). For the sake of comparison, we plot $L(\omega)$ in the absence of gain (green line and filled circles). The solid lines represent the theoretical predictions obtained by the definition of L, whereas the circles

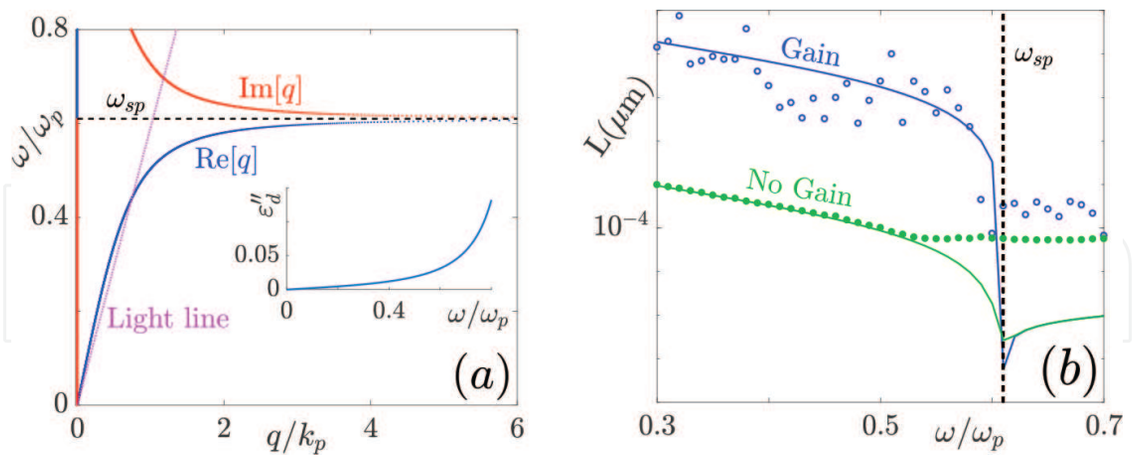

Figure 4. (a) The surface plasmon polariton (SPP) dispersion relation $q(\omega)$ in the presence of a gain material with gain corresponds to lossless SPP propagation. Re[q] and Im[q] are indicated by blue and red lines, respectively. The horizontal dashed black line denotes the SPP frequency ($\omega_{\text{sp}} = 0.61\omega_p$) where an interchanging between Re[q] and Im[q] appears. The dotted magenta line indicates the light line in the dielectric. (Inset) Demonstration of the gain leads to lossless SPP propagation. (b) Theoretical (solid lines) and numerical (circles) prediction of SPP propagation length L in the presence (blue) and in the absence (green) of gain dielectric showing a phase transition that happens at ω_{sp} (vertical dashed black line). Deviations between theoretical and numerical predications for $\omega > \omega_{\text{sp}}$ correspond to quasi-bound EM modes. The $k_p = \omega_p/c$ is used as normalized unit of wavenumbers and ω_p as normalized unit for frequencies.

indicate numerical results. For the numerical calculations, the characteristic propagation length has been estimated by the inverse of the slope of the Log(I), where I is the magnetic intensity along the interface [2–4]. The black vertical dashed line denotes the SPP resonance frequency ω_{sp}, in which the phase transition appears. The graphs in **Figure 4b** indicate that in the presence of the lossless gain, SPPs may travel for very long, practically infinite, distances. Approaching the resonance frequency ω_{sp}, L decreases rapidly leading to a steep phase transition on the SPPs propagation. The deviations between theoretical and numerical results in **Figure 4** for frequencies near and greater than ω_{sp} are attributed to the fact that in the regime $\omega_{\text{sp}} < \omega < \omega_p$, there are quasi-bound EM modes [2, 3], where EM waves are evanescent along the metal-dielectric interface and radiate perpendicular to it. Consequently, the observed EM field for $\omega > \omega_{\text{sp}}$ corresponds to radiating modes [3].

3. Two-dimensional plasmons

In this section, we investigate plasmons in a two-dimensional electron gas (2DEG), where the electron sea is free to move only in two dimensions, tightly confined in the third. The reduced dimensions of electron confinement and Coulomb interaction cause crucial differences in plasmons excitation spectrum. For instance, plasmon spectrum in a 2DEG is gapless in contrast with three-dimensional case [13]. For the sake of completeness, we first discuss briefly plasmons in a regular 2DEG characterized by the usual parabolic dispersion relation (21) for a two-dimensional wavevector $\mathbf{k}$ lies in the plane of 2DEG. Thence, we focus on plasmons in a quite special two-dimensional material, viz. graphene. Graphene is a gapless two-dimensional semi-metal with linear dispersion relation. The linear energy spectrum offers great opportunity to describe graphene with chiral Dirac Hamiltonian for massless spin-1/2 fermions [7, 8, 10]. Furthermore, graphene can be doped with several methods, such as chemical doping [7], by applying an external voltage [10], or with lithium intercalation [16]. The doping shifts the Fermi level toward the conduction bands making graphene a great metal. The advantage to describe graphene electronic properties with massless carriers Dirac equation leads to exceptional optical and electronic properties, like very high electric conductivity and ultra-subwavelength plasmons [6–8, 10].

3.1. Dynamical dielectric function of 2D metals

In order to determine the plasmon spectrum of a two-dimensional electron gas, first of all we calculate the dielectric function in the context of random phase approximation (15) with v_q being the two-dimensional Coulomb interaction of Eq. (16). In the Lindhard formula (23), V and $\mathbf{k}$ denote a two-dimensional volume and wave-vector, respectively. First, we investigate a 2DEG described by the parabolic dispersion relation (21). The electrons are assumed to occupy a single band ignoring interband transitions, that is, transitions to higher bands. Thus, there is no orbital degeneracy $(g_v = 1)$ resulting in the two-dimensional Fermi wavenumber $k_F = \sqrt{2\pi n}$, where n is the carrier (electrons) density [13, 17]. Turning summation (23) into integral by the substitution $V^{-1}\sum_{|\mathbf{k}|}(\ldots) = (2\pi)^{-2}\int d^2\mathbf{k}(\ldots)$, we obtain the Lindhard formula in integral form

$$\chi_0(\mathbf{q},\omega) = \frac{4}{(2\pi)^2}\int d^2|\mathbf{k}|\frac{\varepsilon_{\mathbf{k}+\mathbf{q}} - \varepsilon_{\mathbf{k}}}{(\hbar z)^2 - (\varepsilon_{\mathbf{k}+\mathbf{q}} - \varepsilon_{\mathbf{k}})^2} \tag{54}$$

The singe particle excitation continuum is still defined by expression (25), since the kinetic energy is considered to have the same form as in 3D case, even though the 2D Fermi wavenumber has been modified. Transforming to polar coordinate system (r,θ) and using relation (22), integral (54) reads

$$\chi_0(q,\omega) = \frac{2k_F^3 q}{(2\pi)^2 m z^2}\int_0^1 dx\, x\int_0^{2\pi} d\theta \frac{\frac{q}{k_F} + 2x\cos\theta}{1 - \left(\frac{v_F q}{z}\right)^2\left(\frac{q}{2k_F} + x\cos\theta\right)^2} \tag{55}$$

where x is a dimensionless variable defined as $x = r/k_F$. Previously, since we are interested in long wavelength limit ($q \ll k_F$), we expand the integrand of Eq. (55) around $q = 0$. Keeping up to first orders of q, integral (55) yields

$$\chi_0(q,\omega) = \frac{k_F^2 q^2}{2\pi m\omega^2} \tag{56}$$

where $z \to \omega$ by sending the imaginary part of z to zero. The dielectric function is determined by the formula of Eq. (15) for 2D Coulomb interaction of Eq. (16), hence

$$\varepsilon(q,\omega) = 1 - \frac{2\pi n e^2 q}{m\omega^2} \tag{57}$$

The 2DEG plasmon dispersion relation is determined by Eq. (11) to be

$$\omega_p^{2D}(q) = \sqrt{\frac{2\pi n e^2 q}{m}} \tag{58}$$

related with volume plasmons dispersion relation by $\omega_p^{2D}(q) = \omega_p\sqrt{q/2}$. In contrast to three-dimensional electron gas where plasmon spectrum is gapped, in two-dimensional case the plasmon frequency depends on $\sqrt{q}$ making the plasmon spectrum gapless. In **Figure 2**, the 2D plasmon dispersion relation (58) is demonstrated together with three-dimensional case. Furthermore, it is worth pointing out the similarity between the plasmon dispersion relation of 2DEG of Eq. (58) and SPP of Eq. (44), that is, both show $\sqrt{q}$ dependence.

Let us now investigate the most special two-dimensional electron gas, namely graphene. At the limit where the excitation energy is small compared to E_F, the dispersion relation of graphene, viz. the relation between kinetic energy $\epsilon_{\mathbf{k}}^s$ and momentum $\mathbf{p} = \hbar\mathbf{k}$, is described by two linear bands as

$$\epsilon_{\mathbf{k}}^s = s\hbar v_F|\mathbf{k}| \tag{59}$$

where $s = \pm 1$ indicates the conduction (+1) and valence (-1) band, respectively, v_F is the two-dimensional Fermi velocity which is constant for graphene and equal to $v_F = 10^6$ m/s [7, 8, 10, 16, 18]. Because of valley degeneracy $g_v = 2$, the Fermi momentum is modified to read

$k_F = \sqrt{2\pi n/g_v} = \sqrt{\pi n}$ [8, 18]. The Fermi energy, given by $E_F = \hbar v_F k_F$, becomes zero in the absence of doping ($n = 0$). As a consequence, the E_F crosses the point where the linear valence and conduction bands touch each other, namely at the Dirac point, giving rise to the semimetal character of the undoped graphene [7, 15, 16, 18]. The Lindhard formula of Eq. (19) needs to be generalized to include both intra- and interband transitions (valley degeneracy) as well as the overlap of states, hence

$$\chi_0(\mathbf{q},\omega) = -\frac{g_s g_v}{V}\sum_{s,s'}\sum_{\mathbf{k}}\frac{f(\epsilon^{s'}_{\mathbf{k}+\mathbf{q}}) - f(\epsilon^{s}_{\mathbf{k}})}{\hbar\omega - (\epsilon^{s'}_{\mathbf{k}+\mathbf{q}} - \epsilon^{s}_{\mathbf{k}}) + i\hbar\eta}F_{ss'}(\mathbf{k},\mathbf{k}+\mathbf{q}) \tag{60}$$

where the factors $g_s = g_v = 2$ account to spin and valley degeneracy, respectively. The Lindhard formula has been modified to contain two extra summations $\left(\sum_{s=-1}^{1}\sum_{s'=-1}^{1}\right)$ corresponding to valley degeneracy for the two bands of Eq. (59). In addition, the overlap of states function $F_{ss'}(\mathbf{k},\mathbf{k}+\mathbf{q})$ has been introduced and defined by $F_{ss'}(\mathbf{k},\mathbf{k}+\mathbf{q}) = (1 + ss'\cos\psi)/2$, where ψ is the angle between $\mathbf{k}$ and $\mathbf{k}+\mathbf{q}$ vectors [5, 18]. The term $\cos\psi$ can be expressed in $|\mathbf{k}|$, $|\mathbf{k}+\mathbf{q}|$ and θ terms, and subsequently the overlap function is written as [8]

$$F_{ss'}(\mathbf{k},\mathbf{k}+\mathbf{q}) = \frac{1}{2}\left(1 + ss'\frac{|\mathbf{k}| + |\mathbf{q}|\cos\theta}{|\mathbf{k}+\mathbf{q}|}\right). \tag{61}$$

In long wavelength limit, we approximately obtain

$$|\mathbf{k}+\mathbf{q}| = |\mathbf{k}|\left(1 + \frac{|\mathbf{q}|\cos\theta}{|\mathbf{k}|} + \frac{|\mathbf{q}|^2\sin^2\theta}{2|\mathbf{k}|^2}\right). \tag{62}$$

In this limit, we obtain for the graphene dispersion relation (59) the general form

$$\epsilon^{s}_{\mathbf{k}+\mathbf{q}} - \epsilon^{s'}_{\mathbf{k}} = s\hbar v_F\left(\frac{s-s'}{s}|\mathbf{k}| + |\mathbf{q}|\left(\cos\theta + \frac{|\mathbf{q}|}{2|\mathbf{k}|}\sin^2\theta\right)\right). \tag{63}$$

In turn, the plasmon-damping regimes are determined by the poles of polarizability (60) by substituting expression (63). Due to the valley degeneracy, there are two damping regimes corresponding, respectively, to intraband ($s = s'$)

$$\omega < v_F q \tag{64}$$

and interband ($s = -s'$)

$$v_F(2k_F - q) < \omega < v_F(2k_F + q). \tag{65}$$

electron-hole pair excitations [8] demonstrated in **Figure 5** by shaded areas.

Substituting the long wavelength limit expression (62) in the overlap function (61), the latter reads

http://dx.doi.org/10.5772/67900

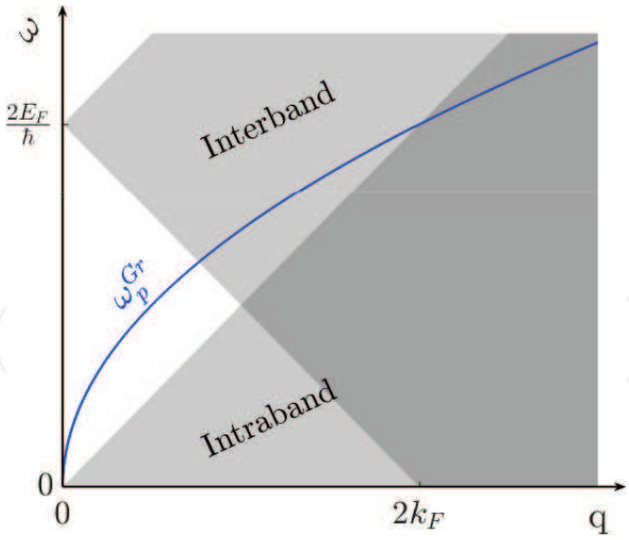

Figure 5. Blue solid line indicates the dispersion relation of graphene plasmons (ω_p^{Gr}). The shaded regimes represent the intra- and interband Landau damping where plasmon decays to electron-hole pairs excitation.

$$F_{ss'}(\mathbf{k},\mathbf{k}+\mathbf{q}) = \begin{cases} 1-\dfrac{q^2}{4k^2}\sin^2\theta & \simeq 1 \quad s=s' \text{ (intraband)} \\ \dfrac{q^2}{4k^2}\sin^2\theta & \simeq 0 \quad s\neq s' \text{ (interband)} \end{cases} \tag{66}$$

Equation (66) states that in long wavelength limit, the interband contribution can be neglected [5], hence, the Lindhard formula (60) is simplified to

$$\chi_0(\mathbf{q}\to 0,\omega) = -\frac{4}{V}\sum_{\mathbf{k}}\left\{\frac{f(\epsilon^+_{\mathbf{k}+\mathbf{q}})-f(\epsilon^+_{\mathbf{k}})}{\hbar z-(\epsilon^+_{\mathbf{k}+\mathbf{q}}-\epsilon^+_{\mathbf{k}})}+\frac{f(\epsilon^-_{\mathbf{k}+\mathbf{q}})-f(\epsilon^-_{\mathbf{k}})}{\hbar z-(\epsilon^-_{\mathbf{k}+\mathbf{q}}-\epsilon^-_{\mathbf{k}})}\right\}. \tag{67}$$

As it has already been mentioned, in zero temperature limit, the Fermi-Dirac distribution $f(\epsilon^{\pm}_{\mathbf{k}})$ is simplified to Heaviside step function $\Theta(k_F \mp |\mathbf{k}|)$. In this limit, the second term in the right hand of Eq. (67) is always zero, since $\Theta(k_F+|\mathbf{k}|)=\Theta(k_F+|\mathbf{k}+\mathbf{q}|)=1$, which reflects that all states in the valence band are occupied. Making again the elementary transformation $\mathbf{k}+\mathbf{q}\to-\mathbf{k}$ in the term of Eq. (67) that includes $f(\epsilon^+_{\mathbf{k}+\mathbf{q}})$, we obtain

$$\chi_0(\mathbf{q}\to 0,\omega) = \frac{8}{V}\sum_{|\mathbf{k}|<k_F}\frac{\epsilon^+_{\mathbf{k}+\mathbf{q}}-\epsilon^+_{\mathbf{k}}}{(\hbar z)^2-(\epsilon^+_{\mathbf{k}+\mathbf{q}}-\epsilon^+_{\mathbf{k}})^2}. \tag{68}$$

Turning summation (68) into integral, we read

$$\chi_0(\mathbf{q}\to 0,\omega) = \frac{8}{(2\pi)^2}\int d^2|\mathbf{k}|\frac{\epsilon^+_{\mathbf{k}+\mathbf{q}}-\epsilon^+_{\mathbf{k}}}{(\hbar z)^2-(\epsilon^+_{\mathbf{k}+\mathbf{q}}-\epsilon^+_{\mathbf{k}})^2}. \tag{69}$$

Transforming to polar coordinates for $r=|\mathbf{k}|$ and using relation (63), we obtain the integral

$$\chi_0(\mathbf{q},\omega) = \frac{2E_F k_F q}{\pi^2\hbar^2\omega^2}\int_0^1 dx \int_0^{2\pi} \frac{x\cos\theta + \frac{q}{2k_F}\sin^2\theta}{1-\left(\frac{v_F q}{\omega}\right)^2\left(\cos\theta + \frac{q}{2k_F x}\sin^2\theta\right)^2} d\theta, \tag{70}$$

where $x = r/k_F$, $q = |\mathbf{q}|$ and $\eta = 0 \Rightarrow z = \omega$. In non-static ($\omega \gg v_F q$) and long wavelength ($q \ll k_F$) limits, we expand the integrator of Eq. (69) in series of q. Keeping up to first power of q/k_F, we obtain

$$\chi_0(\mathbf{q}\to 0,\omega) = \frac{2E_F k_F q}{\pi^2\hbar^2\omega^2}\int_0^1 dx \int_0^{2\pi} \left(x\cos\theta + \frac{q}{2k_F}\sin^2\theta\right) d\theta. \tag{71}$$

The evaluation of integral (71) is trivial and leads to the polarizability function of graphene

$$\chi_0(\mathbf{q}\to 0,\omega) = \frac{E_F}{\pi\hbar^2}\frac{q^2}{\omega^2}. \tag{72}$$

Using the RPA formula (15), we obtain the long wavelength dielectric function of graphene

$$\varepsilon(q,\omega) = 1 - \frac{2e^2 E_F}{\hbar^2\omega^2} q \tag{73}$$

indicating that at low energies doped graphene is described by a Drude-type dielectric function with plasma frequency depending straightforward on the doping amount, namely the Fermi energy level E_F. The plasma frequency of graphene monolayer is determined by condition (11) and reads

$$\omega_p^{Gr}(q) = \sqrt{\frac{2e^2 E_F}{\hbar^2} q} \tag{74}$$

indicating the $q^{1/2}$ dependence likewise plasmons at a regular 2DEG. The most important result is the presence of $\hbar$ in the denominator of Eq. (74), which reveals that plasmons in graphene are purely quantum modes, that is, there are no classical plasmons in doped graphene. In addition, graphene plasmon frequency is proportional to $n^{1/4}$, which is different from classical 2D plasmon behavior where $\omega_p^{2D} \sim n^{1/2}$ [7, 18]. This is a direct consequence of the quantum relativistic nature of graphene, since Fermi energy is defined differently in any case, namely $E_F \sim k_F \sim n^{1/2}$ in graphene, whereas, $E_F \sim k_F^2 \sim n$ in 2DEG case. In **Figure 3(a)**, we represent the plasmon dispersion relation in doped graphene.

3.2. Graphene plasmonic metamaterial

Multilayers of plasmonic materials have been used for designing metamaterials providing electromagnetic propagation behavior not found under normal circumstances like negative refraction and epsilon-near-zero (ENZ) [9, 19, 20]. The bottleneck in creating plasmonic devices with

any desirable characteristic has been the limitations of typical 3D solids in producing perfect interfaces for the confinement of electrons and the features of dielectric host. This may no longer be a critical issue. The advent of truly two-dimensional materials like graphene (a metal), transition-metal dichalcogenides (TMDC's, semiconductors), and hexagonal boron nitride (hBN, an insulator) makes it possible to produce structures with atomic-level control of features in the direction perpendicular to the stacked layers [9, 21]. This is ushering a new era in manipulating the properties of plasmons and designing devices with extraordinary behavior.

Here, we propose a systematic method for constructing epsilon-near-zero (ENZ) metamaterials by appropriate combination on 2D materials. The aforementioned metamaterials exhibit interesting properties like diffractionless EM wave propagation with no phase delay [9]. We show analytically that EM wave propagation through layered heterostructures can be tuned dynamically by controlling the operating frequency and the doping level of the 2D metallic layers. Specifically, we find that multilayers of a plasmonic 2D material embedded in a dielectric host exhibit a plasmonic Dirac point (PDP), namely a point in wavenumber space where two linear coexisting dispersion curves cross each other, which, in turn, leads to an effective ENZ behavior [9]. To prove the feasibility of this design, we investigate numerically EM wave propagation in periodic plasmonic structures consisting of 2D metallic layers lying on yz plane in the form of graphene, arranged periodically along the x axis and possessing surface conductivity σ_s. The layers are embedded in a uniaxial dielectric host in the form of TMDC or hBN multilayers of thickness d and with uniaxial relative permittivity tensor $\overline{\overline{\varepsilon}}_d$ with diagonal components $\varepsilon_x \neq \varepsilon_y = \varepsilon_z$. We explore the resulting linear, elliptical, and hyperbolic EM dispersion relations which produce ENZ effect, ordinary and negative diffraction, respectively.

We solve the analytical problem under TM polarization, with the magnetic field parallel to the y direction which implies that there is no interaction of the electric field with ε_y. We consider a magnetically inert (relative permeability $\mu = 1$) lossless host ($\varepsilon_x, \varepsilon_z \in \mathbb{R}$). For monochromatic harmonic waves in time, the Maxwell equations lead to three equations connecting the components of the **E** and **H** fields. For the longitudinal component [9, 19], $E_z = (\mathrm{i}\eta_0/k_0\varepsilon_z)(\partial H_y/\partial x)$ where $\eta_0 = \sqrt{\mu_0/\varepsilon_0}$ is the free space impedance. Defining the vector of the transversal field components as $\psi = (E_x, H_y)^T$ gives [9]

$$\mathrm{i}\frac{\partial}{\partial z}\psi = k_0\eta_0 \begin{pmatrix} 0 & 1+\frac{1}{k_0^2}\frac{\partial}{\partial_x}\frac{1}{\varepsilon_z}\frac{\partial}{\partial_x} \\ \frac{\varepsilon_x}{\eta_0^2} & 0 \end{pmatrix}\psi \tag{75}$$

Assuming EM waves propagating along the z axis, viz. $\psi(x,z) = \psi(x)e^{\mathrm{i}k_z z}$, Eq. (75) leads to an eigenvalue problem for the wavenumber k_z of the plasmons along z [9, 19]. The metallic 2D planes are assumed to carry a surface current $J_s = \sigma_s E_z$, which acts as a boundary condition in the eigenvalue problem. Furthermore, infinite number of 2D metals are considered to be arranged periodically, along x axis, with structural period d. The magnetic field reads $H_y^-(x)e^{\mathrm{i}k_z z}$ for $-d < x < 0$ and $H_y^+(x)e^{\mathrm{i}k_z z}$ for $0 < x < d$ on either side of the metallic plane at $x = 0$, with boundary conditions $H_y^+(0) - H_y^-(0) = \sigma_s E_z(0)$ and $\partial_x H_y^+(0) = \partial_x H_y^-(0)$. Due to the

periodicity, we use Bloch theorem along x as $H_y^+(x) = H_y^-(x-d)e^{\mathrm{i}k_x d}$, with Bloch wavenumber k_x. As a result, we arrive at the dispersion relation [9, 19, 20]:

$$F(k_x,k_z) = \cos(k_x d) - \cosh(\kappa d) + \frac{\xi\kappa}{2}\sinh(\kappa d) = 0 \tag{76}$$

where $\kappa^2 = (\varepsilon_z/\varepsilon_x)(k_z^2 - k_0^2\varepsilon_x)$ expresses the anisotropy of the host medium and $\xi = -(\mathrm{i}\sigma_s\eta_0/k_0\varepsilon_z)$ coincides with the so-called "plasmonic thickness" which determines the SPP decay length [9, 19, 20]. In particular, ξ is twice the SPP penetration length and defines the maximum distance between two metallic layers where the plasmons are strongly interacting [9, 19, 20]. We point out that for lossless 2D metallic planes σ_s is purely imaginary and ξ is purely real (for $\varepsilon_z \in \mathbb{R}$). At the center of the first Brillouin zone $k_x = 0$, the equation has a trivial solution [19] for $\kappa = 0 \Rightarrow k_z = k_0\sqrt{\varepsilon_x}$ which corresponds to the propagation of x-polarized fields travelling into the host medium with refractive index $\sqrt{\varepsilon_x}$ without interacting with the 2D planes which are positioned along z axis [22]. Near the Brillouin zone center ($k_x/k_0 \ll 1$ and $\kappa \simeq 0$) and under the assumption of a very dense grid ($d \to 0$), we obtain $k_x d \ll 1$ and $\kappa d \ll 1$, we Taylor expand the dispersion equation (76) to second order in d, hence

$$\frac{k_z^2}{\varepsilon_x} + \frac{d}{(d-\xi)\varepsilon_z}k_x^2 = k_0^2. \tag{77}$$

The approximate relation (77) is identical to that of an equivalent homogenized medium described by dispersion: $k_z^2/\varepsilon_x^{\mathrm{eff}} + k_x^2/\varepsilon_z^{\mathrm{eff}} = k_0^2$ [9, 21]. Subsequently, from a metamaterial point of view, the entire system is treated as a homogeneous anisotropic medium with effective relative permittivities given by

$$\varepsilon_x^{\mathrm{eff}} = \varepsilon_x\ ,\ \varepsilon_z^{\mathrm{eff}} = \varepsilon_z + \mathrm{i}\frac{\eta_0\sigma_s}{k_0 d} = \varepsilon_z\frac{d-\xi}{d}. \tag{78}$$

We read from Eq. (78) the capability to control the behavior of the overall structure along the z direction. For instance, the choice $d = \varepsilon_z/(\varepsilon_z - \varepsilon_x)\xi$ leads to an isotropic effective medium with $\varepsilon_z^{\mathrm{eff}} = \varepsilon_x^{\mathrm{eff}}$ [9].

For the lossless case ($\mathrm{Im}[\xi] = 0$), we identify two interesting regimes, viz. the strong plasmon coupling for $d < \xi$ and the weak plasmon coupling for $d > \xi$. In both cases, plasmons develop along z direction at the interfaces between the conducting planes and the dielectric host. In the strong coupling case ($d < \xi$), plasmons of adjacent interfaces interact strongly with each other. As a consequence, the shape of the supported band of Eq. (77), in the (k_x,k_z) plane, is hyperbolic (dashed red line in **Figure 6(a)**) and the system behaves as a hyperbolic metamaterial [9, 19, 22] with $\varepsilon_x^{\mathrm{eff}} > 0$, $\varepsilon_z^{\mathrm{eff}} < 0$. On the other hand, in the weak plasmon coupling ($d > \xi$), the interaction between plasmons of adjacent planes is very weak. In this case, the shape of the dispersion relation (77) on the (k_x,k_z) plane is an ellipse (dotted black line in **Figure 6(a)**) and the systems act as an ordinary anisotropic media with $\varepsilon_z^{\mathrm{eff}}, \varepsilon_x^{\mathrm{eff}} > 0$ [9]. We note that in the case $\xi < 0$ the system does not support plasmons and the supported bands are always ellipses [9]. When either the 2D medium ($\mathrm{Re}[\sigma_s] \neq 0$) or the host material is lossy, a similar separation holds by replacing ξ by $\mathrm{Re}[\xi]$.

http://dx.doi.org/10.5772/67900

The most interesting case is the linear dispersion, where k_z is linearly dependent on k_x and dk_x/dk_z is constant for a wide range of k_z [9, 19]. When this condition holds, the spatial harmonics travel with the same group velocity into the effective medium [9, 19]. To engineer our structure to exhibit a close-to-linear dispersion relation, we inspect the approximate version of Eq. (77): a huge coefficient for k_x will make k_0^2 on the right-hand-side insignificant; if $\xi = d$, the term proportional to k_x^2 increases without bound yielding a linear relation between k_z and k_x. With this choice, $\sigma_s = -\mathrm{i}(k_0 d\varepsilon_z/\eta_0)$, and substituting in the exact dispersion relation Eq. (76), we find that $(k_x,k_z) = (0,k_0\sqrt{\varepsilon_x})$ becomes a saddle point for the transcendental function $F(k_x,k_z)$ giving rise to the conditions for the appearance of two permitted bands, namely two lines on the (k_x,k_z) plane across which $F(k_x,k_z) = 0$. This argument connects a mathematical feature, the saddle point of the dispersion relation, with a physical feature, the crossing point of the two coexisting linear dispersion curves, the plasmonic Dirac point [9] (solid blue line in **Figure 6(a)**). From a macroscopic point of view, the choice $\xi = d$ makes the effective

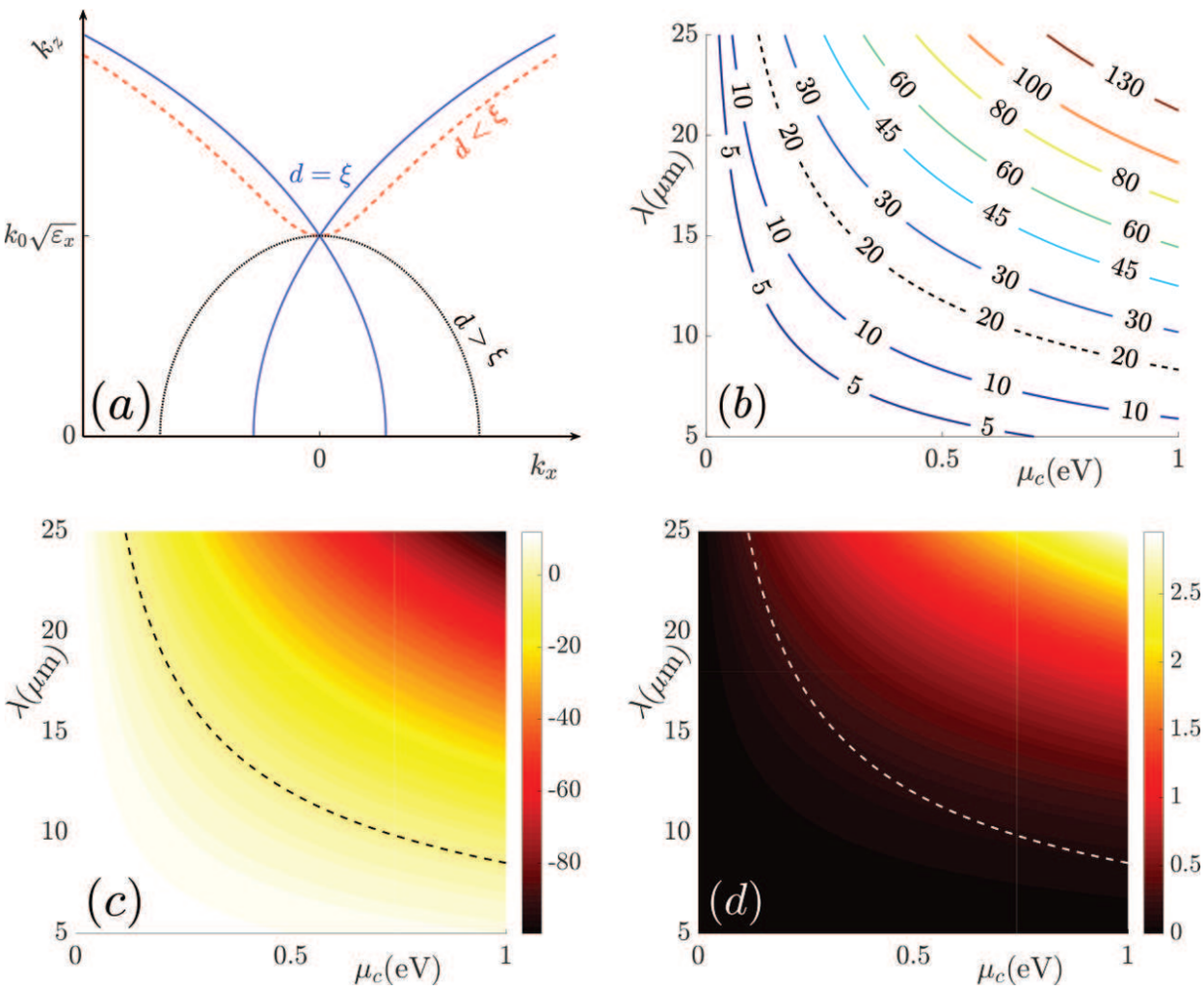

Figure 6. (a) The three supported dispersion plasmonic bands in (k_x,k_z) plane: hyberbolic (dashed red), elliptical (dotted black), and linear (solid blue) where plasmonic Dirac point (PDP) appears. (b) Combinations of graphene doping μ_c and free-space operational wavelengths λ leading to epsilon-near-zero (ENZ) behavior (PDP in dispersion relation) for several lattice periods d (in nm). (c) Real and (d) imaginary parts of the effective permittivity $\varepsilon_z^{\mathrm{eff}}$ for the choice $d = 20$ nm (dashed line in (b)); dashed curves indicate the ENZ regime.

permittivity along the z direction vanish, as is evident from Eq. (78). As a result, the existence of a PDP makes the effective medium behave like an ENZ material in one direction ($\varepsilon_z^{\text{eff}} = 0$).

The plasmonic length ξ is, typically, restricted in few nanometers ($\xi < 100$ nm). Regular dielectrics always present imperfections in nanoscales, hence, the use of regular materials as dielectric hosts is impractical. Furthermore, graphene usually exfoliates or grows up on other 2D materials. Because of the aforementioned reasons, it is strongly recommended that the dielectric host to be also a 2D material with atomic scale control of the thickness d and no roughness. For instance, one could build a dielectric host by stacking 2D layers of materials molybdenum disulfide (MoS_2) [23] with essentially perfect planarity, complementing the planarity of graphene.

Substituting the graphene dielectric function (73) into formula (18), we calculate the two-dimensional Drude-type conductivity of graphene [6, 19, 21]

$$\sigma_s(\omega) = \frac{\mathrm{i}e^2\mu_c}{\pi\hbar^2(\omega + \mathrm{i}/\tau)}, \tag{79}$$

where μ_c is the tunable chemical potential equal to Fermi energy E_F and τ is the transport-scattering time of the electrons [6, 19] introduced in the same manner as in Eq. (30). In what follows, we use bulk MoS_2, which at THz frequencies is assumed lossless with a diagonal permittivity tensor of elements, $\varepsilon_x \cong 3.5$ (out of plane) and $\varepsilon_y = \varepsilon_z \cong 13$ (in plane) [23].

The optical losses of graphene are taken into account using $\tau = 0.5$ ps [19]. Since the optical properties of the under-investigated system can be controlled by tuning the doping amount, the operating frequency or the structural period, in **Figure 6(b)**, we show proper combinations of μ_c and operational wavelength in free space λ which lead to a PDP for several values of lattice density distances ($d = \mathrm{Re}[\xi]$ in nm) [9]. To illustrate, for a reasonable distance between successive graphene planes of $d = 20$ nm, the real (**Figure 6(c)**) and imaginary (**Figure 6(d)**) effective permittivity values that can be emulated by this specific graphene-MoS_2 architecture determine the device characteristics at different frequencies and graphene-doping levels. Positive values of $\mathrm{Re}[\varepsilon_z^{\text{eff}}]$ are relatively moderate and occur for larger frequencies and lower doping levels of graphene; on the other hand, $\mathrm{Im}[\varepsilon_z^{\text{eff}}]$ is relatively small in the ENZ region as indicated by a dashed line in both graphs [9]. On the other hand, losses become larger as $\mathrm{Re}[\varepsilon_z^{\text{eff}}]$ gets more negative.

To examine the actual electromagnetic field distribution in our graphene-MoS_2 configuration, we simulate the EM wave propagation through two finite structures consisting of 40 and 100 graphene planes with $\mathrm{Re}[\xi] = 20.8$ nm and for operational wavelength in vacuum $\lambda = 12$ m ($f = 25$ THz $=$ 0.1 eV). In order to have a complete picture of the propagation properties, we excite the under-investigating structures with a 2D dipole magnetic source as well as with a TM plane wave source. In particular, the 40-layered structure is excited by a 2D magnetic dipole source, which is positioned close to one of its two interfaces and oriented parallel to them, denoted by a white dot in **Figure 7(a)–(c)**. On the other hand, the 100-layered configuration is excited by a plane source, which is located below the multilayer and is rotated by 20^o

http://dx.doi.org/10.5772/67900

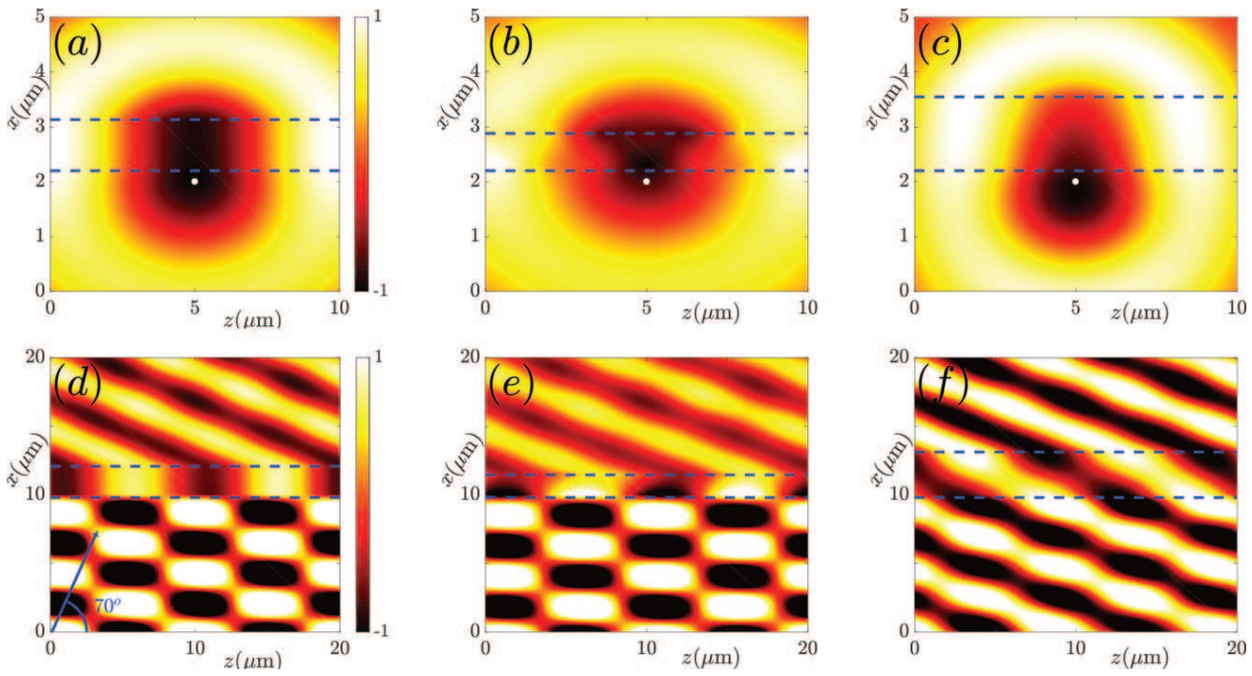

Figure 7. Spatial distribution of the magnetic field (color map) of graphene-MoS_2 multilayer structure located between the blue dashed lines and embedded in MoS_2 background. In (a)–(c), the metamaterial consists of 40 graphene sheets and excited by a magnetic dipole (white dot). In (d)–(f), the structure is composed by 100 graphene layers and excited by a TM plane wave source located at $y = 0$ and rotated 20^o with respect to the interface. (a), (d) $d = \mathrm{Re}[\xi]$ (ENZ behavior). (b), (e) $d = 0.7\mathrm{Re}[\xi]$ hyperbolic metamaterial. (c), (f) $d = 1.5\mathrm{Re}[\xi]$ elliptical medium, where $\mathrm{Re}[\xi] = 20.8\,\mathrm{nm}$. Due to high reflections in (d), (e), we observe pattern formation of stationary waves below the metamaterial.

with respect to the interface; the blue arrow in **Figure 7(d)** indicates the direction of the incident wave. The normalized to one spatial distribution of the magnetic field value is shown in **Figure 7** in color representation, where the volume containing the graphene multilayers is between the dashed blue lines. To minimize the reflections, the background region is filled with a medium of the same dielectric properties as MoS_2. In **Figure 7(a** and **d)**, the system is in the critical case ($d = \mathrm{Re}[\xi]$), where the waves propagate through the graphene sheets without dispersion as in an ENZ medium. In **Figure 7(b** and **e)**, the interlayer distance is $d = 0.7\mathrm{Re}[\xi]$ (strong plasmon-coupling regime) and the system shows negative (anomalous) diffraction. In **Figure 7(c** and **f)** $d = 1.5\mathrm{Re}[\xi]$ (weak plasmon-coupling regime) and the EM wave show ordinary diffraction through the graphene planes [9].

4. Conclusion

In summary, we have studied volume and surface plasmons beyond the classical plasma model. In particular, we have described electronic excitations in solids, such as plasmons and their damping mechanism, viz. electron-hole pairs excitation, in the context of the quantum approach random phase approximation (RPA), a powerful self-consistent theory for determining the dielectric function of solids including screening non-local effect. The dielectric function and, in turn, the plasmon dispersion relation have been calculated for a bulk metal, a two-dimensional electron gas (2DEG) and for graphene, the famous two-dimensional semi-metal.

The completely different dispersion relation between plasmon in three- and two-dimensional metals has been pointed out. Furthermore, we have highlighted the fundamental difference between plasmons in a regular 2DEG and in doped graphene, indicating that plasmons in graphene are purely quantum modes, in contrast to plasmons in 2DEG, which originate from classical laws. Moreover, the propagation properties of surface plasmon polariton (SPP), a guided collective oscillation mode, have been also investigated. For the completeness of our theoretical investigation, we have outlined two applications. First, we have examined SPPs properties along an interface consisting of a bulk metal and an active (gain) dielectric. We have found that there is a gain value for which the metallic losses have been completely eliminated resulting in lossless SPP propagation. Second, we have investigated a plasmonic metamaterial composed of doped graphene monolayers. We have shown that depending on operating frequency, doping amount, and interlayer distance between adjacent graphene layers, the wave propagation properties present epsilon-near-zero behavior, normal, and negative refraction, providing a metamaterial with tunable optical properties.

Acknowledgements

We acknowledge discussions with D. Massatt and E. Manousakis and partial support by the European Union under programs H2020-MSCA-RISE-2015-691209-NHQWAVE and by the Seventh Framework Programme (FP7-REGPOT-2012-2013-1) under grant agreement no. 316165. We also acknowledge support by EFRI 2-DARE NSF Grant No. 1542807 (M.M); ARO MURI Award No. W911NF14-0247 (E.K.). We used computational resources on the Odyssey cluster of the FAS Research Computing Group at Harvard University.

Author details

Marios Mattheakis[1,2]*, Giorgos P. Tsironis[2] and Efthimios Kaxiras[1,3]

*Address all correspondence to: mariosmat@g.harvard.edu

1 School of Engineering and Applied Sciences, Harvard University, Cambridge, MA, USA

2 Department of Physics, University of Crete, Heraklion, Greece

3 Department of Physics, Harvard University, Cambridge, MA, USA

References

[1] Kittel C. Introduction to Solid State Physics. 8th ed. USA: John Wiley & Sons, Inc; 2005. 680 p.

[2] Maier SA. Plasmonics: Fundamentals and Applications. New York: Springer; 2007. 223 p.

[3] Mattheakis M, Oikonomou T, Molina MI, Tsironis GP. Phase transition in PT symmetric active plasmonic systems. IEEE J. Sel. Top. Quantum Electron. 2016;**22**:5000206. DOI: 10.1109/JSTQE.2015.2490018

[4] Pitarke JM, Silkin VM, Chulkov EV, Echenique PM. Theory of surface plasmons and surface-plasmon-polaritons. Rep. Pro. Phys. 2007;**70**:1–87. DOI: 10.1088/0034-4885/70/1/R01

[5] Kenneth W, Shung K. Dielectric function and plasmon structure of stage-1 intercalated graphite. Phys. Rev. B. 1986;**34**:979–993. DOI: 10.1103/PhysRevB.34.979

[6] Jablan M, Buljan H, Soljačić M. Plasmonics in graphene at infrared frequencies. Phys. Rev. B. 2009;**80**:245435. DOI: 10.1103/PhysRevB.80.245435

[7] Grigorenko AN, Polini M, Novoselov KS. Graphene plasmonics. Nat. Photon. 2012;**6**:749–758. DOI: 10.1038/NPHOTON.2012.262

[8] Gonçalves PAD, Peres NMR. An Introduction to Graphene Plasmonics. World Scientific Publishing, Singapore; 2016. 431 p.

[9] Mattheakis M, Valagiannopoulos CA, Kaxiras E. Epsilon-near-zero behavior from plasmonic Dirac point: Theory and realization using two-dimensional materials. Phys. Rev. B. 2016;**94**:201404(R). DOI: 10.1103/PhysRevB.94.201404

[10] Fei Z, Rodin AS, Andreev GO, Bao W, McLeod AS, Wagner M, Zhang LM, Zhao Z, Thiemens M, Dominguez G, Fogler MM, Castro Neto AH, Lau CN, Keilmann F, and Basov DN. Gate-tuning of graphene plasmons revealed by infrared nano-imaging. Nature. 2012;**487**:82–85. DOI: 10.1038/nature11253

[11] March NH, Parrinello M. Collective Effects in Solids and Liquids. Bristol: Adam Hilger LTD; 1982. pp. 4–45.

[12] Isihara A. Electron Liquids. 2nd ed. Berlin, Germany: Springer; 1998. pp. 21–36.

[13] Monarkha Y, Kono K. Two-Dimensional Coulomb Liquids and Solids. Berlin, Germany: Springer; 2004. pp. 65–103.

[14] Psaltakis GC. Quantum Many-Particle Systems. Heraklion: Crete University Press; 2012. 707 p. (In Greek)

[15] Kaxiras E. Atomic and Electronic Structure of Solids. New York, USA: Cambridge University Press; 2003. 676 p.

[16] Shirodkar SN, Mattheakis M, Cazeaux P, Narang P, Soljačic′ M, Kaxiras E. Visible quantum plasmons in lithium-intercalcated multilayer graphene (to be published in 2017). arXiv: 1703.01558

[17] Stern F. Polarizability of a two-dimensional electron gas. Phys. Rev. Let. 1967;**18**:546–548. DOI: 10.1103/PhysRevLett.18.546

[18] Hwang EH, Das Sarma S. Dielectric function, screening, and plasmons in two-dimensional graphene. Phys. Rev. B. 2007;**75**:205418. DOI: 10.1103/PhysRevB.75.205418

[19] Wang B, Zhang X, García Vidal FJ, Yuan X, Teng J. Strong coupling of surface plasmon polaritons in monolayer graphene sheet arrays. Phys. Rev. Lett. 2012;**109**:073901. DOI: 10.1103/PhysRevLett.109.073901

[20] Wang B, Zhang X, Loh KP, Teng J. Tunable broadband transmission and phase modulation of light through graphene multilayers. J. Appl. Phys. 2014;**115**:213102. DOI: 10.1063/1.4880336

[21] Nefedov IS, Valagiannopoulos CA, Melnikov LA. Perfect absorption in graphene multilayers. J. Optics. 2013;**15**:114003. DOI: 10.1088/2040-8978/15/11/114003

[22] Valagiannopoulos CA, Mirmoosa MS, Nefedov IS, Tretyakov SA, Simovski CR. Hyperbolic-metamaterial antennas for broadband enhancement of dipole emission to free space. J. Appl. Phys. 2014;**116**:163106. DOI: 10.1063/1.4900528

[23] Defo RK, Fang S, Shirodkar SN, Tritsaris GA, Dimoulas A, Kaxiras E. Strain dependence of band gaps and exciton energies in pure and mixed transition-metal dichalcogenides. Phys. Rev. B. 2016;**94**:155310. DOI: 10.1103/PhysRevB.94.155310